CAUCHY – Jurnal Matematika Murni dan Aplikasi
Volume 11 (1) (2026), Pages 956-969
p-ISSN: 2086-0382; e-ISSN: 2477-3344

Higher-Order Numerical Solution of the KdV-BBM Equation: A Comparative Analysis of Temporal Integration Schemes in the Method of Lines Framework

Dita Ardiana[1], Ummu Habibah[1*], Trisilowati[1], and Rahifa Binti Ranom[2]

[1]*Department of Mathematics, Brawijaya University, Jl. Veteran, Malang, 65145, East Java, Indonesia*
[2]*Faculty of Electrical Engineering, Universiti Teknikal Malaysia Melaka, 81310, Melaka, Malaysia*

Abstract

This study investigates the numerical simulation of solitary wave propagation governed by the KdV-BBM equation using a robust Method of Lines (MOL) framework. The governing nonlinear equation is transformed into a system of ordinary differential equations through spatial discretization. We evaluate the performance of three temporal integration schemes: the first-order Euler method, the fourth-order Runge-Kutta (RK-4), and the fifth-order iRK-5 method. Quantitative analysis via Mean Absolute Error (MAE) for various time steps ($\Delta t = 0.2, 0.1, 0.05$, and 0.01) reveals that the iRK-5 scheme provides enhanced temporal precision, achieving error magnitudes as low as 10^{-6} and consistently aligning with the exact traveling-wave solution. Notably, the iRK-5 method demonstrates greater algorithmic efficiency; it achieves an accuracy level of 4.55×10^{-6} at a coarser time step of $\Delta t = 0.1$, whereas the RK-4 scheme requires a finer time step of $\Delta t = 0.05$ to reach the same precision. Both high-order methods eventually reach a spatial error floor where further temporal refinement yields no significant reduction in MAE. These findings emphasize that high-order temporal integration, particularly the iRK-5 scheme, is essential for preserving the physical integrity of complex nonlinear wave phenomena while maintaining optimal computational effort.

Keywords: Improved fifth-order Runge-Kutta (iRK-5); KdV-BBM equation; method of lines (MOL); solitary wave propagation.

1. Introduction

The Korteweg-de Vries-Benjamin-Bona-Mahony (KdV-BBM) equation is a critical nonlinear mathematical model in fluid mechanics, particularly for describing the propagation of long waves in dispersive media. Analogous to how Korteweg-type fluid models are extensively utilized to describe complex two-phase fluid flows with capillary effects [1], the KdV-BBM equation combines the dispersive characteristics of the KdV equation with the regularization features of the BBM equation, making it numerically more stable for modeling shallow water waves. However, the inherent nonlinearity and the presence of high-order dispersive terms pose significant challenges. While specific exact solutions, such as solitary and elliptic waves, can be identified under certain conditions [2, 3], a general closed-form analytical solution is often unattainable

*Corresponding author. E-mail: ummu_habibah@ub.ac.id

Submitted: March 11, 2026 Reviewed: April 04, 2026 Accepted: April 12, 2026
DOI: https://doi.org/10.18860/cauchy.v11i1.41525

[4]. This limitation has driven the development of various numerical methods to obtain accurate approximate solutions [5, 6], a necessity frequently encountered when modeling practical fluid dynamics, such as the use of finite difference approaches to simulate real-world river flows [7].

One of the most flexible and well-established approaches for solving partial differential equations (PDEs) is the Method of Lines (MOL). The primary advantage of MOL lies in its ability to transform a PDE into a system of ordinary differential equations (ODEs) through spatial discretization [8]. [9] affirmed the validity and stability of MOL, demonstrating that the resulting ODE system is a legitimate representation of the original PDE, where accuracy increases consistently with the number of discretization lines. Mikhail also clarified that instabilities often attributed to MOL usually originate from the nature of the original equation rather than the method itself. The effectiveness of MOL continues to be proven in recent research; for instance, [10] successfully implemented an MOL scheme with third-order finite differences to solve the Burgers-Huxley equation. In the context of spatial discretization, the use of central finite difference remains a primary choice due to its non-dissipative nature, and it has been proven effective in yielding minimal numerical errors for various boundary value differential problems [11]. Even in the latest technological trends, [12] utilized centered finite differences as a fundamental foundation for modern machine learning-based computational methods on coarse grids.

The success of an MOL scheme in providing precise solutions heavily depends on the choice of temporal integration. The Euler method is often used as an initial benchmark due to its simplicity and computational efficiency [13–15], yet it suffers from strict stability limits in long-term simulations. As an improvement, the fourth-order Runge-Kutta (RK-4) method has become a popular standard due to its balance between computational cost and accuracy [16, 17]. It has explicitly demonstrated higher accuracy and smaller errors when solving ODEs derived from semi-discrete fluid equations, such as the Saint-Venant model and Schrödinger-KdV [18, 19].

To achieve higher precision without sacrificing computational efficiency, the use of higher-order methods is crucial. [20] recently introduced an improved fifth-order Runge-Kutta (iRK-5) method designed to enhance numerical fidelity for initial value problems. The mathematical advantage of the iRK-5 formulation lies in its optimized Taylor series expansion, where the free parameters in the five-stage Butcher tableau are strategically selected to minimize the principal truncation error coefficients. By satisfying a more comprehensive set of order conditions compared to traditional fifth-order schemes, this method achieves a significant reduction in local truncation errors per step. Such refinement is particularly suited for dispersive wave equations like the KdV-BBM, as it suppresses the artificial numerical oscillations and error accumulation that often degrade the solitary wave profile during long-term integration.

Building upon these developments, this study aims to conduct a comparative study between the Euler, RK-4, and iRK-5 methods (based on the formulation by [20]) within the Method of Lines framework to solve the KdV-BBM equation. By applying central finite difference for spatial discretization, this research will evaluate how each temporal integration method affects the stability, convergence rate, and efficiency in preserving the solitary wave profile of the KdV-BBM model.

The remainder of this paper is organized as follows. Section 2 details the numerical methodology, including the spatial discretization using finite differences and the implementation of the Euler, RK-4, and improved iRK-5 temporal integration schemes. In Section 3, we present the results and discussion, focusing on the parametric role analysis of the KdV-BBM equation and a comparative performance evaluation of the numerical schemes through solitary wave simulations. Finally, Section 4 concludes the paper by summarizing the key findings and the implications of the higher-order numerical approach for solitary wave integrity.

2. Methods

This study employs a computational and numerical research design aimed at solving the nonlinear Korteweg-de Vries-Benjamin-Bona-Mahony (KdV-BBM) equation. The core contribu-

tion of this work is a comparative analysis of different temporal integration schemes within the framework of the Method of Lines (MOL). The methodology is structured to provide a clear pathway from the continuous mathematical model to a fully discretized system, ensuring that the results are reproducible and the numerical procedures are transparent.

The mathematical setting of this research involves a nonlinear partial differential equation that incorporates effects from convection, dispersion, and regularization. The study assumes a one-dimensional spatial domain $[x_1, x_N]$ with non-periodic boundary conditions to accurately represent a solitary wave profile. Specifically, we impose time-dependent Dirichlet boundary conditions derived from the analytical solution, $u(x_1, t) = g_1(t)$ and $u(x_N, t) = g_2(t)$. This ensures that the boundary values remain consistent with the exact traveling-wave profile as it evolves.

To provide a mathematically consistent closure for the higher-order spatial derivatives, we additionally employ zero-gradient Neumann conditions, $\partial u/\partial x = 0$, at both boundaries. This numerical closure is essential for determining the values of ghost points (u_0 and u_{N+1}) required by the central difference approximation of the dispersive terms without introducing additional unknowns into the system. The primary analytical challenge addressed is the coupling between the time-dependent term and the mixed space-time derivative, which characterizes the Benjamin-Bona-Mahony component of the equation.

2.1. Spatial Finite Difference Scheme

For the numerical procedure, we adopt the Method of Lines to separate the spatial and temporal discretizations. In the spatial dimension, a second-order central finite difference scheme is employed to approximate the derivatives. According to Schiesser [8], the first and third spatial derivatives at a grid point x_i are discretized as:

$$(u_x)_i \approx \frac{u_{i+1} - u_{i-1}}{2\Delta x}, \quad (u_{xxx})_i \approx \frac{u_{i+2} - 2u_{i+1} + 2u_{i-1} - u_{i-2}}{2(\Delta x)^3}. \tag{1}$$

Furthermore, the second-order derivative involved in the regularization term is given by:

$$(u_{xx})_i \approx \frac{u_{i+1} - 2u_i + u_{i-1}}{(\Delta x)^2}. \tag{2}$$

where I is the identity matrix and D_2 represents the second-order differentiation matrix. A significant part of the numerical algorithm involves solving the linear system at each time step to isolate the temporal evolution of the wave amplitude. This step is necessitated by the regularization term in the KdV-BBM model [9]. Since the operator $(I - \gamma D_2)$ possesses a tridiagonal structure, the system is solved efficiently using specialized tridiagonal solvers rather than direct matrix inversion. This approach minimizes the computational overhead per time step while maintaining the stability required to resolve the dispersive effects of the equation.

2.2. Parametric Role Analysis

During the numerical simulation, special attention is given to the roles of the physical parameters α, β, and γ. These constants govern the balance of the wave dynamics as follows:

- Nonlinearity (α): Controls the steepening of the wave front due to convective effects.
- Dispersion (β): Influences the spreading of the wave and the formation of oscillatory tails.
- Regularization (γ): Acts as a smoothing mechanism that counters high-frequency oscillations, a characteristic feature of the BBM-type equations compared to standard KdV models.

The simulations will demonstrate how variations in these parameters alter the solitary wave's velocity, amplitude, and stability across the different integration schemes.

2.3. Time Integration via Higher-Order Schemes

The time integration of the resulting system, $\frac{d\vec{u}}{dt} = \vec{G}(\vec{u})$, is conducted using three distinct methods. We evaluate three integration methods to advance the solution from t_n to t_{n+1} with a time step Δt. In this study, the time-step Δt is selected based on empirical numerical observations to ensure stability and suppress non-physical oscillations.

2.3.1. Euler Method

The first-order explicit Euler method [13] is defined as:

$$\vec{u}^{n+1} = \vec{u}^n + h\vec{G}(t_n, \vec{u}^n). \tag{3}$$

2.3.2. Fourth-Order Runge-Kutta (RK-4) Method

The standard RK-4 method [16] is given by:

$$\begin{aligned}
\vec{k}_1 &= h\vec{G}(t_n, \vec{u}^n),\\
\vec{k}_2 &= h\vec{G}(t_n + \frac{h}{2}, \vec{u}^n + \frac{\vec{k}_1}{2}),\\
\vec{k}_3 &= h\vec{G}(t_n + \frac{h}{2}, \vec{u}^n + \frac{\vec{k}_2}{2}),\\
\vec{k}_4 &= h\vec{G}(t_n + h, \vec{u}^n + \vec{k}_3),\\
\vec{u}^{n+1} &= \vec{u}^n + \frac{1}{6}(\vec{k}_1 + 2\vec{k}_2 + 2\vec{k}_3 + \vec{k}_4).
\end{aligned} \tag{4}$$

2.3.3. Improved Fifth-Order Runge-Kutta (iRK-5) Method

The novel approach in this study is the Improved RK5 method proposed by Habibah et al. [20]. The scheme is defined as:

$$\vec{u}^{n+1} = \vec{u}^n + \frac{1}{6}\vec{k}_1 + \frac{1}{3}\vec{k}_2 + \frac{1}{3}\vec{k}_3 + \frac{1}{10}\vec{k}_4 + \frac{1}{15}\vec{k}_5, \tag{5}$$

where the intermediate stages are:

$$\begin{aligned}
\vec{k}_1 &= h\vec{G}(t_n, \vec{u}^n),\\
\vec{k}_2 &= h\vec{G}\left(t_n + \frac{h}{2}, \vec{u}^n + \frac{\vec{k}_1}{2}\right),\\
\vec{k}_3 &= h\vec{G}\left(t_n + \frac{h}{2}, \vec{u}^n + \frac{\vec{k}_2}{2}\right),\\
\vec{k}_4 &= h\vec{G}\left(t_n + h, \vec{u}^n + \vec{k}_3\right),\\
\vec{k}_5 &= h\vec{G}\left(t_n + h, \vec{u}^n + \frac{\vec{k}_1}{2} + \frac{\vec{k}_4}{2}\right).
\end{aligned}$$

2.4. Implementation and Validation

All numerical implementations were developed using a Matlab-based computational environment, leveraging optimized libraries for matrix algebra and linear system solvers. To evaluate the precision and convergence of the proposed iRK-5 scheme against the Euler and RK-4 methods, the global numerical error is quantified using the Mean Absolute Error (MAE). The MAE is calculated across the discrete spatial grid at a specific time T as follows:

$$MAE = \frac{1}{N+1}\sum_{i=1}^{N} |u_i^{num} - u_i^{exact}|,$$

where $N+1$ represents the total number of spatial grid points, u_i^{num} is the numerical solution obtained from the integration schemes, and u_i^{exact} is the analytical solution of the KdV-BBM equation at the corresponding point.To ensure reproducibility, the computational tools and environment variables are documented, and the source code is hosted in a dedicated public repository[1].

3. Results and Discussion

This section evaluates the numerical performance of the proposed Method of Lines (MOL) schemes by simulating the propagation of a solitary wave governed by Eq. (6). We analyze the qualitative behavior and quantitative accuracy of the Euler, RK-4, and iRK-5 methods. Consider the KdV-BBM equation given by Eq. (6)

$$u_t + u_x - \gamma u_{xxt} + \beta u_{xxx} + \alpha u u_x = 0, \tag{6}$$

with boundary conditions

$$u(x_1, t) = g_1(t), \qquad u(x_N, t) = g_2(t),$$

where $g_1(t)$ and $g_2(t)$ are the values of the analytical profile at the boundaries. Additionally, to close the higher-order spatial discretization, we employ zero-gradient Neumann conditions as numerical boundary closures.

$$\frac{\partial u}{\partial x}(x_1, t) = 0, \qquad \frac{\partial u}{\partial x}(x_N, t) = 0.$$

The initial condition associated with KdV-BBM Eq. (6) is given by:

$$u(x, 0) = A\,\mathrm{sech}^2(Bx). \tag{7}$$

The exact traveling-wave solution to the KdV-BBM equation is given by Eq. (8).

$$u(x, t) = A\,\mathrm{sech}^2\left(B(x - vt)\right), \tag{8}$$

where A and B are given as follows:

$$A = \frac{3(v-1)}{\alpha} \qquad \text{and} \qquad B = \frac{1}{2}\sqrt{\frac{v-1}{\gamma v + \beta}}.$$

To ensure the solution is well-defined and real-valued, we restrict the parameter space to $\alpha, \beta, \gamma > 0$ and a propagation velocity $v > 1$. Under these conditions, the wave amplitude A and the pulse width parameter B remain positive real constants, ensuring a physically meaningful solitary wave profile.

3.1. Spatial Discretization and System of ODEs Formulation

The initial phase of the MOL involves the approximation of spatial derivatives in Eq. (6) through second-order central finite differences. Specifically, the nonlinear, dispersive, and dissipative terms are discretized as defined in Eqs. (1)–(2), respectively. Substituting Eqs. (1)–(2) into Eq. (6), and approximating u by u_i, we obtain

$$\begin{aligned}\frac{du_i}{dt} = &- \frac{u_{i+1} - u_{i-1}}{2\Delta x} + \gamma \frac{d}{dt}\left(\frac{u_{i+1} - 2u_i + u_{i-1}}{\Delta x^2}\right) - \beta \frac{u_{i+2} - 2u_{i+1} + 2u_{i-1} - u_{i-2}}{2\Delta x^3} \\ &- \alpha u_i \left(\frac{u_{i+1} - u_{i-1}}{2\Delta x}\right).\end{aligned} \tag{9}$$

[1]Source code and configuration files are available at the official project repository.

Eq. (9) can be rearranged into

$$-\frac{\gamma}{\Delta x^2}\frac{du_{i-1}}{dt}+\left(1+\frac{2\gamma}{\Delta x^2}\right)\frac{du_i}{dt}-\frac{\gamma}{\Delta x^2}\frac{du_{i+1}}{dt}=-\frac{1}{2\Delta x}(u_{i+1}-u_{i-1})-\frac{\beta}{2\Delta x^3}(u_{i+2}-2u_{i+1}+2u_{i-1}-u_{i-2})-\frac{\alpha}{2\Delta x}u_i(u_{i+1}-u_{i-1}). \tag{10}$$

Equation (10) is multiplied by Δx^2 to obtain a simpler form as follows.

$$-\gamma\frac{du_{i-1}}{dt}+\left(\Delta x^2+2\gamma\right)\frac{du_i}{dt}-\gamma\frac{du_{i+1}}{dt}=-\frac{\Delta x}{2}(u_{i+1}-u_{i-1})-\frac{\beta}{2\Delta x}(u_{i+2}-2u_{i+1}+2u_{i-1}-u_{i-2})-\frac{\alpha\Delta x}{2}u_i(u_{i+1}-u_{i-1}). \tag{11}$$

Eq. (11) is to be resolved for $i=2,3,\ldots,N-1$. For $i=1$ and $i=N$, the values are known from the boundary conditions.
For $i=2$,

$$-\gamma\frac{du_1}{dt}+(\Delta x^2+2\gamma)\frac{du_2}{dt}-\gamma\frac{du_3}{dt}=-\frac{\Delta x}{2}(u_3-u_1)-\frac{\beta}{2\Delta x}(u_4-2u_3+2u_1-u_0)-\frac{\alpha\Delta x}{2}u_2(u_3-u_1). \tag{12}$$

At the left boundary ($\frac{\partial u_1}{\partial x}=0$), this yields $\frac{u_2-u_0}{2\Delta x}=0$, which implies the ghost-point relation $u_0=u_2$. When the time-dependent Dirichlet condition $u(x_1,t)=g_1(t)$ is used, its temporal derivative $\frac{du_1}{dt}=g_1'(t)$ is determined analytically. Eq. (12) becomes

$$(\Delta x^2+2\gamma)\frac{du_2}{dt}-\gamma\frac{du_3}{dt}=-\frac{\Delta x}{2}(u_3-u_1)-\frac{\beta}{2\Delta x}(u_4-2u_3+2u_1-u_2)-\frac{\alpha\Delta x}{2}u_2(u_3-u_1)+\gamma g_1'(t).$$

For $i=3$,

$$-\gamma\frac{du_2}{dt}+(\Delta x^2+2\gamma)\frac{du_3}{dt}-\gamma\frac{du_4}{dt}=-\frac{\Delta x}{2}(u_4-u_2)-\frac{\beta}{2\Delta x}(u_5-2u_4+2u_2-u_1)-\frac{\alpha\Delta x}{2}u_3(u_4-u_2).$$

$$\vdots$$

For $i=N-2$,

$$-\gamma\frac{du_{N-3}}{dt}+(\Delta x^2+2\gamma)\frac{du_{N-2}}{dt}-\gamma\frac{du_{N-1}}{dt}=-\frac{\Delta x}{2}(u_{N-1}-u_{N-3})-\frac{\beta}{2\Delta x}(u_N-2u_{N-1}+2u_{N-3}-u_{N-4})-\frac{\alpha\Delta x}{2}u_{N-2}(u_{N-1}-u_{N-3}).$$

For $i=N-1$

$$-\gamma\frac{du_{N-2}}{dt}+(\Delta x^2+2\gamma)\frac{du_{N-1}}{dt}-\gamma\frac{du_N}{dt}=-\frac{\Delta x}{2}(u_N-u_{N-2})-\frac{\beta}{2\Delta x}(u_{N+1}-2u_N+2u_{N-2}-u_{N-3})-\frac{\alpha\Delta x}{2}u_{N-1}(u_N-u_{N-2}). \tag{13}$$

Similarly, at the right boundary ($\frac{\partial u_N}{\partial x} = 0$), the condition $\frac{u_{N+1}-u_{N-1}}{2\Delta x} = 0$ leads to $u_{N+1} = u_{N-1}$. When the time-dependent Dirichlet condition $u(x_N, t) = g_2(t)$ is used, its temporal derivative $\frac{du_N}{dt} = g_2'(t)$ is determined analytically. Eq. (13) becomes

$$-\gamma\frac{du_{N-2}}{dt} + (\Delta x^2 + 2\gamma)\frac{du_{N-1}}{dt} = -\frac{\Delta x}{2}(u_N - u_{N-2}) - \frac{\beta}{2\Delta x}(u_{N-1} - 2u_N + 2u_{N-2} - u_{N-3}) - \frac{\alpha\Delta x}{2}u_{N-1}(u_N - u_{N-2}) + \gamma g_2'(t).$$

This system of equations can be written in matrix form as follows.

$$\underbrace{\begin{bmatrix} (\Delta x^2+2\gamma) & -\gamma & 0 & 0 & \cdots & 0 & 0 & 0 & 0 \\ -\gamma & (\Delta x^2+2\gamma) & -\gamma & 0 & \cdots & 0 & 0 & 0 & 0 \\ \vdots & \vdots & \vdots & \vdots & \cdots & \vdots & \vdots & \vdots & \vdots \\ 0 & 0 & 0 & 0 & \cdots & 0 & -\gamma & (\Delta x^2+2\gamma) & -\gamma \\ 0 & 0 & 0 & 0 & \cdots & 0 & 0 & -\gamma & (\Delta x^2+2\gamma) \end{bmatrix}}_{A} \underbrace{\begin{bmatrix} \frac{du_2}{dt} \\ \frac{du_3}{dt} \\ \vdots \\ \frac{du_{N-2}}{dt} \\ \frac{du_{N-1}}{dt} \end{bmatrix}}_{\frac{d\vec{u}}{dt}}$$

$$= \underbrace{\begin{bmatrix} -\frac{\Delta x}{2}(u_3 - u_1) - \frac{\beta}{2\Delta x}(u_4 - 2u_3 + 2u_1 - u_2) - \frac{\alpha\Delta x}{2}u_2(u_3 - u_1) + \gamma g_1'(t) \\ -\frac{\Delta x}{2}(u_4 - u_2) - \frac{\beta}{2\Delta x}(u_5 - 2u_4 + 2u_2 - u_1) - \frac{\alpha\Delta x}{2}u_3(u_4 - u_2) \\ \vdots \\ -\frac{\Delta x}{2}(u_{N-1} - u_{N-3}) - \frac{\beta}{2\Delta x}(u_N - 2u_{N-1} + 2u_{N-3} - u_{N-4}) - \frac{\alpha\Delta x}{2}u_{N-2}(u_{N-1} - u_{N-3}) \\ -\frac{\Delta x}{2}(u_N - u_{N-2}) - \frac{\beta}{2\Delta x}(u_{N-1} - 2u_N + 2u_{N-2} - u_{N-3}) - \frac{\alpha\Delta x}{2}u_{N-1}(u_N - u_{N-2}) + \gamma g_2'(t) \end{bmatrix}}_{f}. \tag{14}$$

Eq. (14) can be simplified to:

$$A\frac{du_i(t)}{dt} = f_i(\vec{u}^{(t)}, t), \quad i = 2, 3, \ldots, N-1, \tag{15}$$

where $\vec{u}^{(t)} = (u_1^{(t)}, u_2^{(t)}, \ldots, u_N^{(t)})$. The system in Eq. (15) is solved at each time step using an efficient tridiagonal solver based on the Thomas algorithm (a specialized LU factorization for tridiagonal systems) to obtain the temporal derivatives $\frac{du_i}{dt}$. This approach avoids the high computational cost of explicit matrix inversion, ensuring the method remains efficient even for a large number of spatial nodes. Given that the computational domain is sufficiently large, the solitary wave remains far from the boundaries, making $g_1'(t)$ and $g_2'(t)$ negligibly small throughout the simulation.

3.2. Temporal Integration and Comparison of Schemes

Spatial discretization via the MOL transforms the governing KdV-BBM equation into the system of ODEs presented in Eq. (15). To advance this system in the temporal domain, we perform a comparative analysis using three distinct integration schemes. To ensure numerical stability and accurately resolve the wave dynamics, the selection of the time step Δt and spatial grid size Δx is based on empirical numerical observations. These parameters are carefully chosen to prevent non-physical oscillations and maintain the integrity of the dispersive solution throughout the simulation. Specifically, we evaluate the baseline performance of the first-order explicit Euler method, the precision of the fourth-order Runge-Kutta (RK-4) scheme, and the enhanced consistency of the fifth-order improved Runge-Kutta (iRK-5) method proposed by [20]. This approach provides a robust assessment of how each solver handles the interaction between nonlinear and dispersive effects over extended periods.

By applying these schemes to the system defined by Eq. (15), we investigate how each temporal solver handles the coupled nonlinear and dispersive terms over extended simulation periods. The

following discussion examines their respective error accumulations, stability constraints, and overall efficiency in preserving the solitary wave profile $u(x,t)$ as it propagates. Special attention is given to the iRK-5 method's ability to maintain the solitary wave peak with high fidelity over time compared to lower-order schemes, ensuring the physical integrity of the soliton is maintained throughout the computational process.

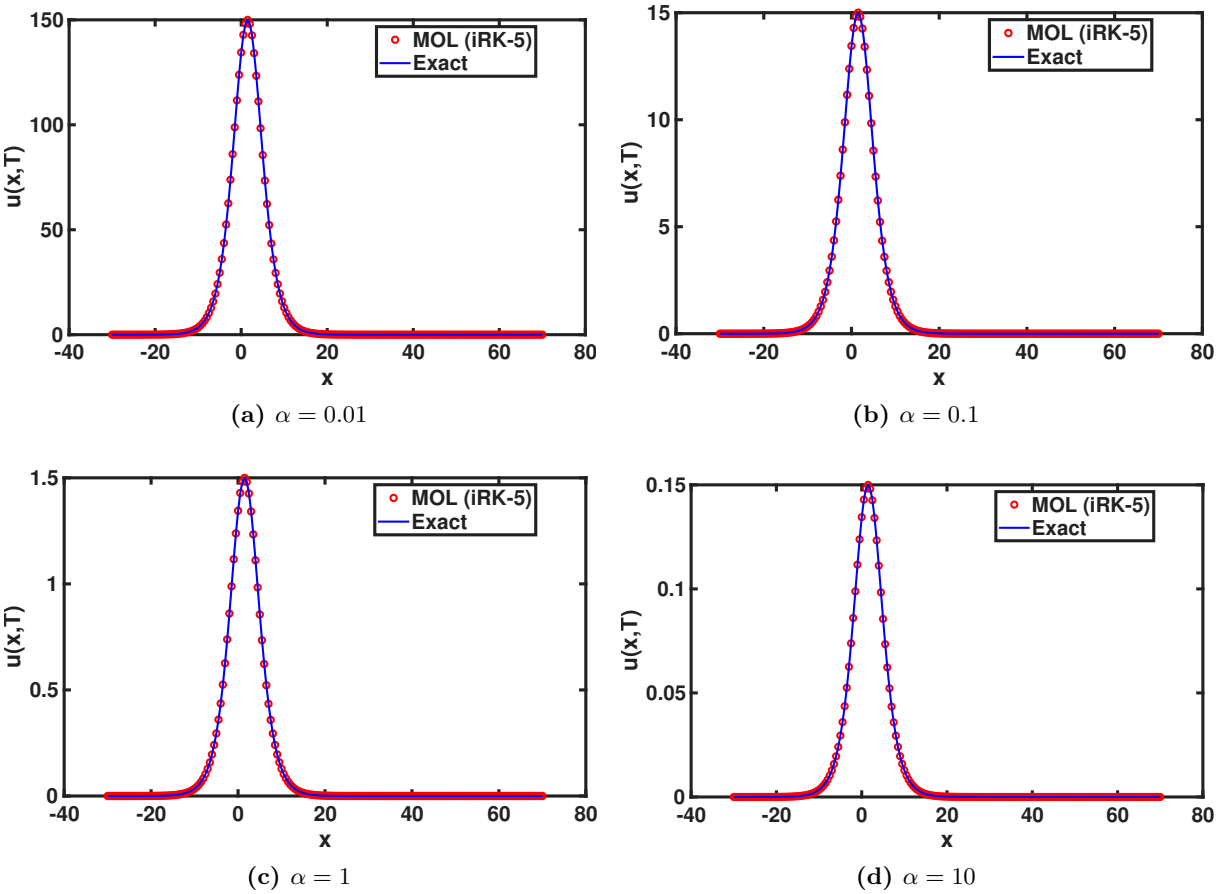

(a) $\alpha = 0.01$ **(b)** $\alpha = 0.1$

(c) $\alpha = 1$ **(d)** $\alpha = 10$

Fig. 1: Exact solution and numerical solution of the KdV-BBM equation with parameters $\beta = 1$, $\gamma = 1$, $v = 1.5$, and various values of α

Based on the visualizations in Fig. 1, the parameter α plays a crucial role in determining the morphology of the solitary wave in the KdV-BBM equation. The nonlinear term $\alpha u u_x$ contributes to the wave-steepening phenomenon, which, in a stable solitary wave, is precisely balanced by the dispersive effects of the β and γ terms. It is observed that the value of α significantly influences the peak amplitude of the resulting wave; for instance, when $\alpha = 0.01$, the system exhibits a high-amplitude profile reaching 150 units, whereas at $\alpha = 10$, the amplitude is reduced to 0.15. This behavior is consistent with the analytical properties of the traveling-wave solution, where the amplitude is inversely related to the nonlinearity coefficient under constant dispersion ($\beta, \gamma = 1$). Despite the amplitude varying across several orders of magnitude, the iRK-5 method consistently maintains the integrity of the solitary wave profile with high precision. This demonstrates the robustness of the numerical scheme in capturing the exact solution across diverse scales of nonlinearity without exhibiting significant numerical oscillations or loss of stability.

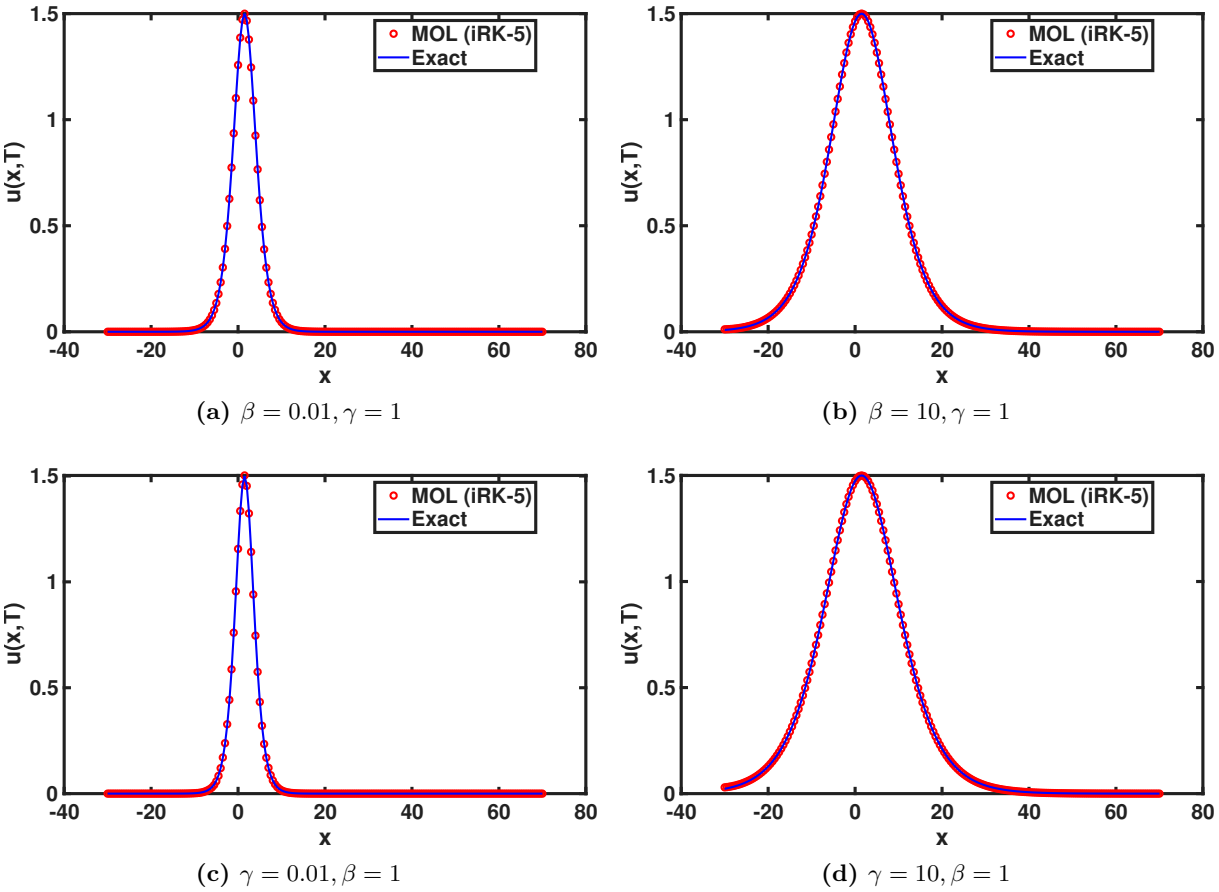

(a) $\beta = 0.01, \gamma = 1$ **(b)** $\beta = 10, \gamma = 1$

(c) $\gamma = 0.01, \beta = 1$ **(d)** $\gamma = 10, \beta = 1$

Fig. 2: Exact solution and numerical solution of the KdV-BBM equation with parameters $\alpha = 1$, $v = 1.5$, and various values of β and γ

Fig. 2 reveals the roles of the dispersion parameters β and γ in determining the wave profile's width and morphology. In contrast to α, which modulates the wave height, changes in β and γ predominantly affect the spatial extent of the solitary wave. As the value of β or γ is increased from 0.01 to 10, the wave undergoes significant widening while maintaining a constant peak amplitude (approximately 1.5 for the $\alpha = 1$ case). This behavior indicates that increasing the dispersive effect leads to a broader wave profile, effectively expanding its spatial domain of influence along the x-axis. The close agreement between the iRK-5 numerical points and the exact traveling-wave solution in Fig. 2 demonstrates the method's capability to accurately capture these dispersive effects across a wide range of wave widths, from narrow to broad structures.

Table 1 presents a comparative analysis between the exact traveling-wave solution and the numerical results obtained using the MOL coupled with three distinct time integration schemes: the first-order Euler method, the fourth-order Runge-Kutta (RK-4), and the fifth-order improved Runge-Kutta (iRK-5). The absolute error distribution shows that the Euler scheme yields the highest discrepancy, consistent with its lower order of accuracy. In contrast, both higher-order methods (RK-4 and iRK-5) significantly reduce the error magnitude to a comparable level, demonstrating improved precision in capturing the solitary wave profile. The near-identical error values observed for RK-4 and iRK-5 suggest that the spatial discretization error ($O(\Delta x^2)$) may have become the dominant source of error at this specific time-step (Δt), thereby masking the theoretical gain in accuracy of the fifth-order integrator. These results highlight the influence of the time integration order on the overall accuracy of the semi-discrete system. The complete numerical data for this analysis are available in the following repository[2].

[2]Data Table 1.

Table 1: Performance Comparison of Euler, RK-4, and iRK-5 Time Integration Schemes within the Method of Lines (MOL) Framework, Including Absolute Error Analysis

x	Exact	MOL(Euler)	MOL(RK-4)	MOL(iRK-5)	Error_{Euler}	Error_{RK-4}	Error_{iRK-5}
−30.000	0.000 005	0.000 001	0.000 002	0.000 002	3.63×10^{-6}	2.67×10^{-6}	2.67×10^{-6}
−29.750	0.000 005	0.000 001	0.000 003	0.000 003	3.62×10^{-6}	2.54×10^{-6}	2.54×10^{-6}
−29.500	0.000 006	0.000 008	0.000 007	0.000 007	1.91×10^{-6}	9.07×10^{-7}	9.07×10^{-7}
−29.250	0.000 006	0.000 004	0.000 004	0.000 004	2.46×10^{-6}	2.39×10^{-6}	2.39×10^{-6}
−29.000	0.000 007	0.000 007	0.000 007	0.000 007	4.58×10^{-7}	1.18×10^{-7}	1.18×10^{-7}
⋮	⋮	⋮	⋮	⋮	⋮	⋮	⋮
−1.000	1.114 050	1.118 918	1.114 640	1.114 640	4.87×10^{-3}	5.90×10^{-4}	5.90×10^{-4}
−0.750	1.176 271	1.183 092	1.176 838	1.176 838	6.82×10^{-3}	5.67×10^{-4}	5.67×10^{-4}
−0.500	1.235 896	1.244 681	1.236 431	1.236 431	8.78×10^{-3}	5.35×10^{-4}	5.35×10^{-4}
−0.250	1.291 876	1.302 563	1.292 371	1.292 371	1.07×10^{-2}	4.95×10^{-4}	4.95×10^{-4}
0.000	1.343 144	1.355 597	1.343 591	1.343 591	1.25×10^{-2}	4.46×10^{-4}	4.46×10^{-4}
0.250	1.388 656	1.402 664	1.389 047	1.389 047	1.40×10^{-2}	3.91×10^{-4}	3.91×10^{-4}
0.500	1.427 431	1.442 713	1.427 758	1.427 759	1.53×10^{-2}	3.27×10^{-4}	3.28×10^{-4}
0.750	1.458 591	1.474 808	1.458 848	1.458 849	1.62×10^{-2}	2.57×10^{-4}	2.57×10^{-4}
1.000	1.481 405	1.498 173	1.481 586	1.481 586	1.68×10^{-2}	1.80×10^{-4}	1.81×10^{-4}
⋮	⋮	⋮	⋮	⋮	⋮	⋮	⋮
69.000	0.000 000	−0.000 005	−0.000 005	−0.000 005	5.38×10^{-6}	4.98×10^{-6}	4.98×10^{-6}
69.250	0.000 000	−0.000 005	−0.000 004	−0.000 004	5.34×10^{-6}	4.20×10^{-6}	4.20×10^{-6}
69.500	0.000 000	−0.000 002	−0.000 001	−0.000 001	1.64×10^{-6}	1.03×10^{-6}	1.03×10^{-6}
69.750	0.000 000	0.000 005	0.000 003	0.000 003	4.98×10^{-6}	3.24×10^{-6}	3.24×10^{-6}
70.000	0.000 000	0.000 007	0.000 005	0.000 005	6.85×10^{-6}	4.55×10^{-6}	4.55×10^{-6}

Table 2: Temporal Error Evolution at Fixed Position $x = -10$ Comparing Euler, RK-4, and iRK-5 Time Integration Schemes within The Method of Lines (MOL) Framework

t	Exact	MOL(Euler)	MOL(RK-4)	MOL(iRK-5)	Error_{Euler}	Error_{RK-4}	Error_{iRK-5}
0.10	0.062 743	0.062 604	0.062 742	0.062 742	1.39×10^{-4}	9.53×10^{-7}	9.50×10^{-7}
0.20	0.058 753	0.058 490	0.058 751	0.058 751	2.62×10^{-4}	1.89×10^{-6}	1.88×10^{-6}
0.30	0.055 011	0.054 639	0.055 008	0.055 008	3.72×10^{-4}	2.79×10^{-6}	2.79×10^{-6}
0.40	0.051 504	0.051 036	0.051 500	0.051 500	4.68×10^{-4}	3.67×10^{-6}	3.66×10^{-6}
0.50	0.048 216	0.047 665	0.048 212	0.048 212	5.51×10^{-4}	4.50×10^{-6}	4.49×10^{-6}
0.60	0.045 135	0.044 512	0.045 130	0.045 130	6.23×10^{-4}	5.29×10^{-6}	5.27×10^{-6}
0.70	0.042 249	0.041 564	0.042 243	0.042 243	6.84×10^{-4}	6.02×10^{-6}	6.01×10^{-6}
0.80	0.039 544	0.038 809	0.039 537	0.039 537	7.35×10^{-4}	6.70×10^{-6}	6.69×10^{-6}
0.90	0.037 010	0.036 233	0.037 003	0.037 003	7.77×10^{-4}	7.33×10^{-6}	7.31×10^{-6}
1.00	0.034 637	0.033 827	0.034 629	0.034 629	8.10×10^{-4}	7.90×10^{-6}	7.88×10^{-6}

Table 2 presented in the table illustrates the numerical stability and accuracy of the MOL at the fixed spatial coordinate $x = -10$ as time t increases from 0.10 to 1.00. A clear trend of error accumulation is evident for all time integration schemes, reflecting the global truncation error inherent in time-stepping procedures. Specifically, the Euler method exhibits a much faster rate of error growth, reaching a magnitude of 8.10×10^{-4} at $t = 1.00$. In comparison, the higher-order RK-4 and iRK-5 schemes demonstrate enhanced precision, maintaining error levels consistently two to three orders of magnitude lower than the Euler approximation (approximately 7.90×10^{-6} and 7.88×10^{-6}, respectively). This confirms that at this spatial point, the higher-order temporal integrators provide a significantly more robust approach for maintaining simulation accuracy over extended durations.

As presented in Table 3, a comparative analysis of the Mean Absolute Error (MAE) and computational efficiency (CPU time) reveals the distinct performance characteristics of the Euler, RK-4, and iRK-5 integration schemes. A critical observation can be made at the largest time step, $\Delta t = 0.20$, where the iRK-5 method achieves a lower MAE (4.5562×10^{-6}) compared to the RK-4 scheme (4.5611×10^{-6}). This indicates that iRK-5 provides enhanced temporal precision and

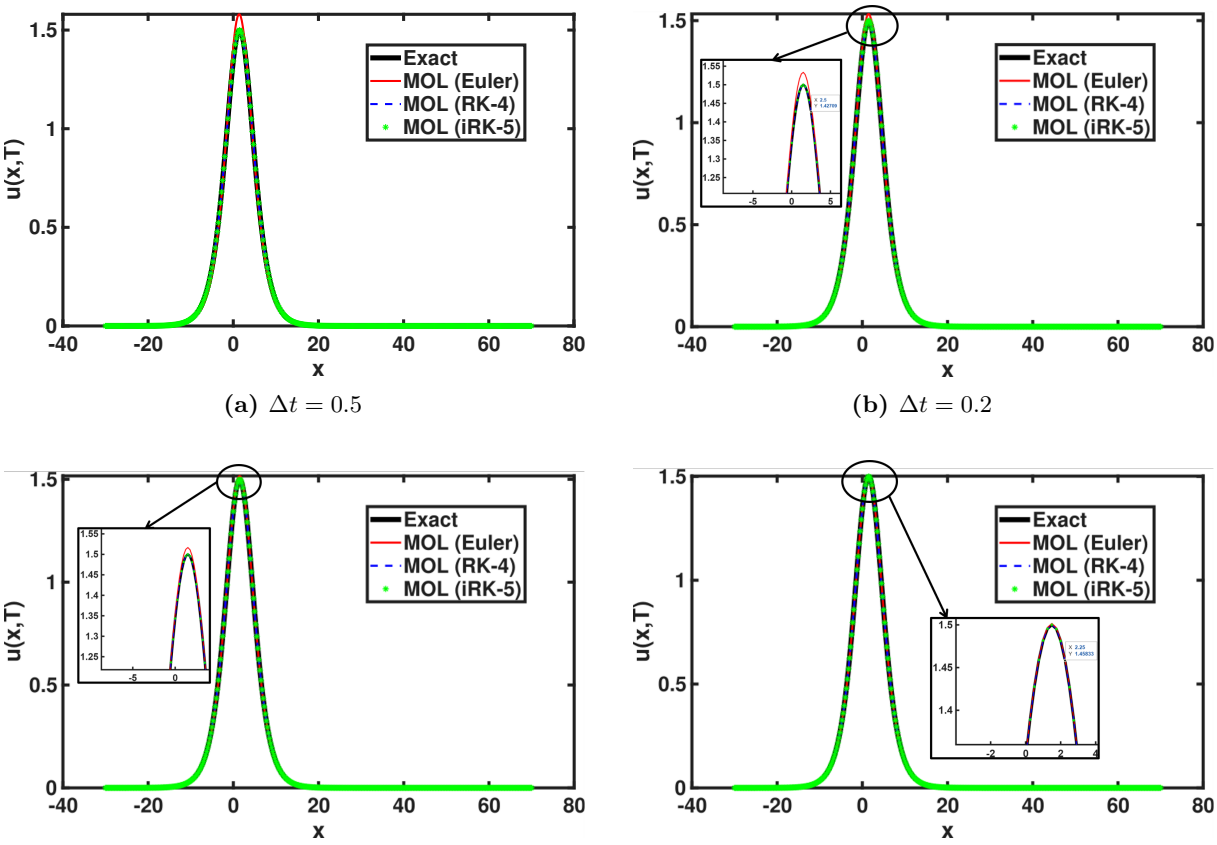

(a) $\Delta t = 0.5$ **(b)** $\Delta t = 0.2$

(c) $\Delta t = 0.1$ **(d)** $\Delta t = 0.01$

Fig. 3: Comparison of solitary wave profiles between the exact solution and numerical solutions using the Method of Lines (MOL) with Euler, RK-4, and iRK-5 time integration schemes at various time steps

Table 3: Comparison of Mean Absolute Error (MAE) for Different Time Steps (Δt) at $T = 1.00$

Δt	MOL(Euler)	MOL(RK-4)	MOL(iRK-5)
0.20	1.0710×10^{-5}	4.5611×10^{-6}	4.5562×10^{-6}
0.10	6.8495×10^{-6}	4.5545×10^{-6}	4.5538×10^{-6}
0.05	5.4640×10^{-6}	4.5538×10^{-6}	4.5537×10^{-6}
0.01	4.7024×10^{-6}	4.5537×10^{-6}	4.5537×10^{-6}
CPU time (s)	0.1958 s	0.4923 s	0.5834 s

more effectively suppresses truncation errors when using coarser time steps. Furthermore, iRK-5 reaches an accuracy level of 4.5538×10^{-6} at $\Delta t = 0.10$, whereas RK-4 requires a finer time step of $\Delta t = 0.05$ to achieve the same result. This suggests that iRK-5 is more algorithmically efficient, as it can maintain high-fidelity solutions with fewer temporal iterations than the standard RK-4.

The data also shows that as Δt is further reduced to 0.01, the MAE for both RK-4 and iRK-5 converges to an identical value of approximately 4.5537×10^{-6}. This plateau signifies that the total numerical error has reached the spatial error floor, which is dictated by the $O(\Delta x^2)$ discretization and the regularization parameter γ. At this stage, the temporal error becomes several orders of magnitude smaller than the spatial error, rendering further temporal refinement redundant. Regarding computational cost, although iRK-5 exhibits a slightly higher CPU time (0.5834 s) due to its five-stage formulation, its improved stability and higher-order consistency at larger time steps justify the minor overhead. This trade-off makes iRK-5 a robust candidate for long-term simulations of the KdV-BBM equation, where maintaining wave integrity at larger time steps is more critical than per-step execution speed.

Fig. 3 visually validates the numerical performance of the three integration schemes across

various time steps. At a larger time step ($\Delta t = 0.5$) in Fig. 3a, the Euler scheme exhibits a noticeable deviation from the solitary wave peak. In contrast, the RK-4 and iRK-5 schemes show a much closer alignment with the exact traveling-wave profile even at this coarser interval. As the time step is refined to $\Delta t = 0.01$, the numerical solutions for all schemes, including Euler, converge toward the exact profile. Notably, the zoomed-in insets reveal that the profiles for RK-4 and iRK-5 are virtually indistinguishable from each other across all tested Δt values. This observation reinforces the earlier suggestion that at finer temporal resolutions, the overall precision is likely limited by spatial discretization errors rather than the temporal integration order. These results demonstrate that while higher-order schemes provide better stability and accuracy at larger time steps, the choice of Δt remains a critical empirical factor in ensuring wave integrity for all methods.

4. Conclusion

This study demonstrates the successful application of the Method of Lines (MOL) to the KdV-BBM equation, confirming that while the physical parameters α, β, and γ dictate the morphology, specifically the amplitude and width of the solitary wave, the choice of time integration scheme is the primary determinant of numerical accuracy. Quantitative results reveal that the first-order Euler method suffers from significant error accumulation, whereas the higher-order RK-4 and iRK-5 schemes achieve significantly lower Mean Absolute Error (MAE), reaching a spatial error floor of approximately 4.55×10^{-6}. Notably, the iRK-5 method demonstrates greater algorithmic efficiency, as it achieves the maximum possible precision at a coarser time step ($\Delta t = 0.1$) compared to the RK-4 scheme, which requires a finer step ($\Delta t = 0.05$). While the Euler method remains stable under refined step sizes, it lacks the high-fidelity accuracy of the Runge-Kutta variants.

The implementation of this MOL framework involves a minor computational trade-off; the necessity of solving the linear system at each time step results in a slightly higher CPU time for the iRK-5 method (0.5834 s) compared to RK-4 (0.4923 s). However, this overhead is justified by the scheme's ability to maintain the integrity of the traveling-wave profile over extended simulation periods. Future research should focus on optimizing the spatial solver to further reduce computational costs. Potential avenues include the use of specialized tridiagonal matrix algorithms or parallel computing techniques to mitigate the computational burden when transitioning to significantly finer spatial grids or higher-dimensional domains.

CRediT Authorship Contribution Statement

Dita Ardiana: Conceptualization, Validation, Methodology, Formal Analysis, Writing-Original draft. **Ummu Habibah:** Conceptualization, Validation, Writing–Review & Editing. **Trisilowati:** Conceptualization, Validation, Writing–Review & Editing. **Rahifa Binti Ranom:** Conceptualization, Validation, Writing–Review & Editing.

Declaration of Generative AI and AI-assisted technologies

During the preparation of this manuscript, the authors utilized the generative AI tool Gemini (Flash 3) to assist in refining the linguistic quality, improving sentence structure, and proofreading the text. The primary role of this technology was to enhance the clarity and formal tone of the academic writing. The authors maintain full responsibility for the intellectual content, technical accuracy, and final interpretation of the results presented in this work.

Declaration of Competing Interest

The authors declare no competing interests.

Funding and Acknowledgments

This research received no external funding.

Data and Code Availability

The dataset and code analyzed during the current study are publicly available in the repository[3].

References

[1] Suma Inna, Muhammad Manaqib, and Ilman Gifari. "Analysis of Korteweg-type compressible fluid model with slip boundary conditions in 3-dimensional half-space". In: *CAUCHY* 9.2 (Nov. 2024), pp. 270–286. DOI: 10.1088/1742-6596/1872/1/012036.

[2] Stefan C Mancas and Ronald Adams. "Elliptic solutions and solitary waves of a higher order KdV–BBM long wave equation". In: *J. Math. Anal. Appl.* 452.2 (2017), pp. 1168–1181. DOI: 10.1016/j.jmaa.2017.03.057.

[3] Rambabu Vana, Perumandla Karunakar, and Ravi Kumar Davala. "Solitary wave solution of the KdV-BBM equation with triangular fuzzy number incorporation". In: *Eng. Comput. (Swansea)* (2025), pp. 1–19. DOI: 10.1108/EC-05-2025-0473.

[4] Nakao Hayashi and Pavel I Naumkin. "Modified scattering for the higher-order KdV–BBM equations". In: *J. Pseudodiffer. Oper. Appl.* 15.1 (2024). DOI: 10.1007/s11868-024-00588-0.

[5] Apipoom Polwang, Kanyuta Poochinapan, and Ben Wongsaijai. "Numerical simulation of wave flow : Integrating the BBM-KdV equation using compact difference schemes". In: *Math. Comput. Simul.* 236 (2025), pp. 70–89. DOI: 10.1016/j.matcom.2025.03.012.

[6] Teeranush Suebcharoen, Kanyuta Poochinapan, and Ben Wongsaijai. "Bifurcation analysis and numerical study of wave solution for initial-boundary value problem of the KdV-BBM equation". In: *Mathematics* 10.20 (2022), p. 3825. DOI: 10.3390/math10203825.

[7] Dian Eka Ratnasari, Meliana Pasaribu, Meliana Pasaribu, Yudhi Yudhi, and Yudhi Yudhi. "Application of the Saint-Venant model for simulation of the Kapuas River flow using the finite difference method". In: *CAUCHY* 11.1 (May 2026), pp. 413–425. DOI: 10.18860/ca.v9i2.29048.

[8] William E. Schiesser. *The Numerical Method of Lines: Integration of Partial Differential Equations*. San Diego, CA: Academic Press, 1991. https://books.google.com/books?id=0_7vAAAAMAAJ.

[9] Mikhail Naguib Mikhail. "On the validity and stability of the method of lines for the solution of partial differential equations". In: *Appl. Math. Comput.* 22.2-3 (1987), pp. 89–98. DOI: 10.1016/0096-3003(87)90038-5.

[10] Muhammad Yaseen, Muhammad Ameer Hamza, Khidir Shaib Mohamed, and Naglaa Mohammed. "A method of lines scheme with third-order finite differences for Burgers–Huxley equation". In: *Axioms* 15.3 (2026), p. 158. DOI: 10.3390/axioms15030158.

[11] Ummu Habibah, Mohamad Handri Tuloli, Viva Rimanada, and Tomas Goncalves Ferreira. "Penyelesaian Numerik Masalah Syarat Batas Robin pada Persamaan Diferensial Cauchy-Euler". In: *mjm* 3.1 (Mar. 2020), pp. 32–40. DOI: 10.36815/majamath.v3i1.615.

[12] Kristina O F Williams and Benjamin F Akers. "Numerical simulation of the Korteweg–de Vries equation with machine learning". In: *Mathematics* 11.13 (2023), p. 2791. DOI: 10.3390/math11132791.

[3] Repository

[13] Emmanuel Hanert, Daniel Y Le Roux, Vincent Legat, and Eric Deleersnijder. "An efficient Eulerian finite element method for the shallow water equations". In: *Ocean Model. (Oxf.)* 10.1-2 (2005), pp. 115–136. DOI: 10.1016/j.ocemod.2004.06.006.

[14] Z Kamont and J Newlin-Łukowicz. "Generalized Euler method for nonlinear first-order partial differential equations". In: *Nonlinear Oscil. (N. Y.)* 6.4 (2003), pp. 444–462. DOI: 10.1023/B:NONO.0000028584.03014.72.

[15] Huang Mingyou and Vidar Thomée. "On the backward Euler method for parabolic equations with rough initial data". In: *SIAM J. Numer. Anal.* 19.3 (1982), pp. 599–603. DOI: 10.1137/0719040.

[16] S Karthick, R Mahendran, and V Subburayan. "Method of lines and Runge-Kutta method for solving delayed one dimensional transport equation". In: *J. Math. Comput. Sci.* 28.03 (2022), pp. 270–280. DOI: 10.22436/jmcs.028.03.05.

[17] Abhijat Sarma, Thomas W Watts, Mudassir Moosa, Yilian Liu, and Peter L McMahon. "Quantum variational solving of nonlinear and multidimensional partial differential equations". In: *Phys. Rev. A (Coll. Park.)* 109.6 (2024). DOI: 10.1103/PhysRevA.109.062616.

[18] M Sukron, U Habibah, and N Hidayat. "Numerical solution of Saint-Venant equation using Runge-Kutta fourth-order method". In: *J. Phys. Conf. Ser.* 1872.1 (May 2021), p. 012036. DOI: 10.18860/cauchy.v11i1.38622.

[19] Yifei Huang, Gang Peng, Gengen Zhang, and Hong Zhang. "High-order Runge–Kutta structure-preserving methods for the coupled nonlinear Schrödinger–KdV equations". en. In: *Math. Comput. Simul.* 208 (June 2023), pp. 603–618. DOI: 10.1016/j.matcom.2023.01.031.

[20] Ummu Habibah, Fermin Franco Medrano, Adith Chandra Permana, Dita Ardiana, and Trisilowati. "An improved fifth-order Runge-Kutta method with higher accuracy and efficiency for solving initial value problems". In: *Sci. Technol. Indones.* 10.3 (2025), pp. 802–816. DOI: 10.26554/sti.2025.10.3.802-816.